A&A 515, A71 (2010)
DOI: 10.1051/0004-6361/200913370

Astronomy & Astrophysics

Vibrationally excited HC_3N in NGC 4418

F. Costagliola⋆ and S. Aalto⋆⋆

Department of Radio and Space Science, Chalmers University of Technology, Onsala Space Observatory, 439 92 Onsala, Sweden
e-mail: [francesco.costagliola;saalto]@chalmers.se

Received 29 September 2009 / Accepted 26 January 2010

ABSTRACT

Aims. We investigate the molecular gas properties of the deeply obscured luminous infrared galaxy NGC 4418. We address the excitation of the complex molecule HC_3N to determine whether its unusually luminous emission is related to the nature of the buried nuclear source.

Methods. We use IRAM 30 m and JCMT observations of rotational and vibrational lines of HC_3N to model the excitation of the molecule by means of rotational diagrams.

Results. We report the first confirmed extragalactic detection of vibrational lines of HC_3N. We detect 6 different rotational transitions ranging from $J = 10$–9 to $J = 30$–29 in the ground vibrational state and obtain a tentative detection of the $J = 38$–37 line. We also detect 7 rotational transitions of the vibrationally excited states v_6 and v_7, with angular momenta ranging from $J = 10$–9 to 28–27. The energies of the upper states of the observed transitions range from 20 to 850 K. In the optically thin regime, we find that the rotational transitions of the vibrational ground state can be fitted for two temperatures, 30 K and 260 K, while the vibrationally excited levels can be fitted for a rotational temperature of 90 K and a vibrational temperature of 500 K. In the inner 300 pc of NGC 4418, we estimate a high HC_3N abundance, of the order of 10^{-7}.

Conclusions. The excitation of the HC_3N molecule responds strongly to the intense radiation field and the presence of warm, dense gas and dust at the center of NGC 4418. The intense HC_3N line emission is a result of both high abundances and excitation. The properties of the HC_3N emitting gas are similar to those found for hot cores in Sgr B2, which implies that the nucleus (<300 pc) of NGC 4418 is reminiscent of a hot core. The potential presence of a compact, hot component ($T = 500$ K) is also discussed.

Key words. galaxies: evolution – globular clusters: individual: NGC 4418 – galaxies: starburst – galaxies: active – radio lines: ISM – ISM: molecules

1. Introduction

Luminous infrared galaxies (LIRGs) are intriguing challenges to modern astronomy. They emit most of their radiation in the infrared (IR) region of the spectrum in the form of dust thermal continuum, and have typical IR luminosities of $L_{\rm IR} > 10^{10}\ L_{\odot}$. In many of these objects, the central power source responsible for the total energy output is buried deep inside the dusty central region and has an origin that remains unclear. For instance, Spoon et al. (2007); Aalto et al. (2007) suggest that dusty, compact LIRGs may represent the early obscured stages of either active galactic nuclei (AGNs) or starbursts and thus play a fundamental role in galaxy formation and evolution.

Owing to the large column of intervening material, observations at IR or shorter wavelengths only detect the surface of the optically thick nuclear regions, where molecular gas column densities can reach values that exceed $N(H_2) = 10^{24}$ cm^{-2}. Thus optical emission becomes completely absorbed by the gas and dust, unless the source geometry allows the emission to escape. These high masses of gas and dust may also cause an AGN to become Compton thick and hard X-rays to become absorbed by the intervening material, adding to problems in identifying the nuclear source. At radio wavelengths, free-free emission from intervening ionized material may also obscure an AGN (e.g., Sanders & Mirabel 1996). This leads to great observational ambiguities that are reflected by the classification of LIRGs varying considerably with the observed frequency band. To produce the high central luminosity observed in many LIRGs requires either an AGN or a nuclear starburst (or a combination of the two) to heat a large volume of dust. Dust temperatures in the inner hundred to a few hundred parsec vary among galaxies and can range from 20–30 K to in excess of 170 K (e.g., Evans et al. 2003; Downes & Eckart 2007). Dissipation of turbulence, which acts on the gas phase (e.g., Guesten et al. 1993) may also indirectly contribute to the heating of dust. Because of the aforementioned large amount of obscuring material, the interplay between the possible energy sources remains difficult to ascertain by direct investigation.

Millimetre observations of molecular lines provide a potentially valuable tool for determining the effects of the central power source on the interstellar medium (ISM) of LIRGs and indirectly constraining some of their key properties, such as gas temperature, density, and chemistry. Chemical models (Meijerink et al. 2007) show how X-ray dominated regions (XDRs), generally expected in the case of accretion onto a central compact object, and photodissociation regions (PDRs), generated by large UV fluxes from young stars, leave different imprints in the ISM composition. The peculiar molecular chemistry of dense hot cores around nascent stars was also described by Viti & Bayet (2008). The gas temperature structure is also expected to be different around an AGN compared to a starburst. For example, in an XDR model bulk gas temperatures can be as high as 200 K, while in a starburst the temperatures should be around 20–50 K (Meijerink et al. 2007).

⋆ F.C. wishes to thank the EU ESTRELA programme for support.
⋆⋆ S.A. wishes to thank the Swedish Research Council for grant support.

Molecular lines surveys of LIRGs, focused mainly on high density tracers, such as HCN, HCO^+, HNC, and CS, have been carried out by several groups (e.g., Krips et al. 2008; Graciá-Carpio et al. 2008; Baan et al. 2008; Imanishi et al. 2007; Gao & Solomon 2004; Aalto et al. 2002). However, even if these studies provide unprecedented insights into the ISM of active galaxies, the interpretation of their results remains debated and more sensitive tracers need to be found.

In surveys of external galaxies (see Sect. 4.5), bright HC_3N J = 10–9 line emission is found in a subset of IR luminous galaxies. The HC_3N line emission is a useful tracer of warm and dense regions and is extremely sensitive to a strong IR-field because of its multiple, mid-IR bending modes. The molecule is often found to be abundant in Galactic hot cores (e.g., de Vicente et al. 2000) and can be easily destroyed by intense UV and particle radiation. Thus HC_3N serves as a tracer of the gas (and dust) properties of galaxies with intense IR fields but where the dense gas is not too exposed to destructive radiation.

The edge-on, Sa-type galaxy NGC 4418 has one of the highest luminosities in HC_3N (relative to HCN) found for an external galaxy so far (Aalto et al. 2007; Monje & Aalto 2008). Its unusual HC_3N emission was first reported by Aalto et al. (2007). The inner region of NGC 4418 is deeply dust-enshrouded (Spoon et al. 2001) with mid-IR intensities that are indicative of dust temperatures of 85 K (Evans et al. 2003) inside a radius of 50 pc. The IR luminosity-to-molecular gas mass ratio is high for a non-ULIRG galaxy indicating that intense, compact activity is hidden behind the dust. Interferometric observations of HCN J = 1–0 by Imanishi et al. (2004) show that the bulk of the dense gas is contained in the inner 2″, corresponding to a region of 300 pc in diameter. NGC 4418 is a FIR-excess galaxy with a logarithmic IR-to-radio continuum ratio (q) of 3 (Roussel et al. 2003). This excess may be caused by either a young pre-supernova starburst or a buried AGN (Aalto et al. 2007; Roussel et al. 2003; Imanishi et al. 2004). The luminous HC_3N signature was interpreted as young starburst activity (Aalto et al. 2007). However we need to perform more detailed observations and modeling of HC_3N emission of NGC 4418 to interpret its origin accurately. A tentative detection of a mm vibrational HC_3N line (Aalto et al. 2007) led us to explore the excitation and abundance of HC_3N in NGC 4418 and search for a model of the dense gas properties in the inner 300 pc of the galaxy. Throughout this paper we assume that the observed HC_3N line emission emerges from a region smaller than or equal to the scale of the interferometric HCN observations by Imanishi et al. (2004).

In this paper, we report the first confirmed extragalactic detections of vibrationally excited HC_3N in the LIRG NGC 4418 with the IRAM 30m telescope. We report in total 13 different transitions of HC_3N – including vibrationally excited levels – allowing us to compile a first model of the excitation and abundance of HC_3N. We also report a tentative detection of the 345 GHz rotational J = 38–37 line with the JCMT telescope. In Sect. 2, we present the observations and results in terms of line intensities. In Sect. 3, we present the results in terms of HC_3N rotational diagrams and, in Sect. 4, we briefly discuss the interpretation of our results and future aims.

2. Observations

The observations were carried out in December 2007 and July 2008 with the IRAM 30 m telescope on Pico Veleta, Spain. The coordinates of the observed position, taken from the NASA/IPAC Extragalactic Database (NED), are $12^h26^m54.6^s$, $-00^d52^m39^s$ (EQ 2000). Calibration scans were taken every five minutes and pointing checked against nearby bright pointing sources every two hours. The nominal pointing accuracy was about 2″, much smaller than the typical full width at half maximum of our beam. For both epochs, observations were performed in wobbler switching mode, with a throw of 120″ and 0.5 Hz phase, to optimize the baseline quality. The backends consisted of two filterbanks of 1 MHz and 4 MHz channel width, connected to the 100 GHz and 230 GHz receivers respectively. The weather conditions in the 2007 run were excellent with precipitable water vapour of 1 mm or less. Even although the summer weather during the 2008 observations led to higher system temperatures, the poorer atmospheric transmission was counterbalanced by deeper integrations, leading to typical rms noise levels of 0.2 mK at 20 km s^{-1} resolution.

In the last observing run, the tuning of the IRAM 30 m receivers was optimized to include the largest possible number of vibrationally excited transitions, and the rotational transition of the vibrational ground state. This allowed us to compare the new data with our previous observations of the vibrational ground state, to exclude possible calibration or baseline errors. By comparing the two datasets, we conclude that the calibration errors are smaller than or equal to 20%.

Data analysis was performed with CLASS[1] and X-Spec[2] software packages. A first order baseline was subtracted from all spectra, which are shown in Fig. 1. The properties of all the HC_3N observed transitions are reported in Table 1, together with main beam efficiencies, transitions probabilities and energies of the upper states.

3. Results

3.1. Detected lines

The rest-frame frequencies of the observed transitions were taken from the NIST database of *Recommended Rest Frequencies for Observed Interstellar Molecular Microwave Transitions*[3] and cross-checked with laboratory and theoretical values from Yamada & Creswell (1986). The notation for the vibrational quantum numbers is in the form J_u-J_l (v_6, v_7), following Yamada & Creswell (1986).

The interaction between the bending angular momentum of the vibrationally excited states and the rotational angular momentum of the molecule, leads to a l-splitting of the levels. Each vibrational state is thus split into two levels, labelled e or f depending on the wavefunction's parity properties. These parity labels are also shown in Table 1. A useful reference for labelling of doubled levels in linear molecules is Brown et al. (1975).

We detected the HC_3N rotational transitions J = 10–9, 16–15, 17–16, 25–24, 28–27, and 30–29. For the J = 10–9, 17–16, 25–24, and 28–27 lines, we also detected rotational transitions of the v_7 = 1 vibrationally excited levels. For the v_6 = 1 lines, we generally have upper limits, the only clear detection being in the J = 25–24 band. The observed HC_3N transitions were selected to minimize blends by major species. We excluded the possibility of blending by radio recombination lines as well as by other molecules (e.g., methanol). The lack of methanol emission is interesting and will be discussed in an upcoming paper.

[1] http://iram.fr/IRAMFR/GILDAS/
[2] http://www.chalmers.se/rss/oso-en/observations/data-reduction-software
[3] http://physics.nist.gov/PhysRefData/Micro/Html/contents.html

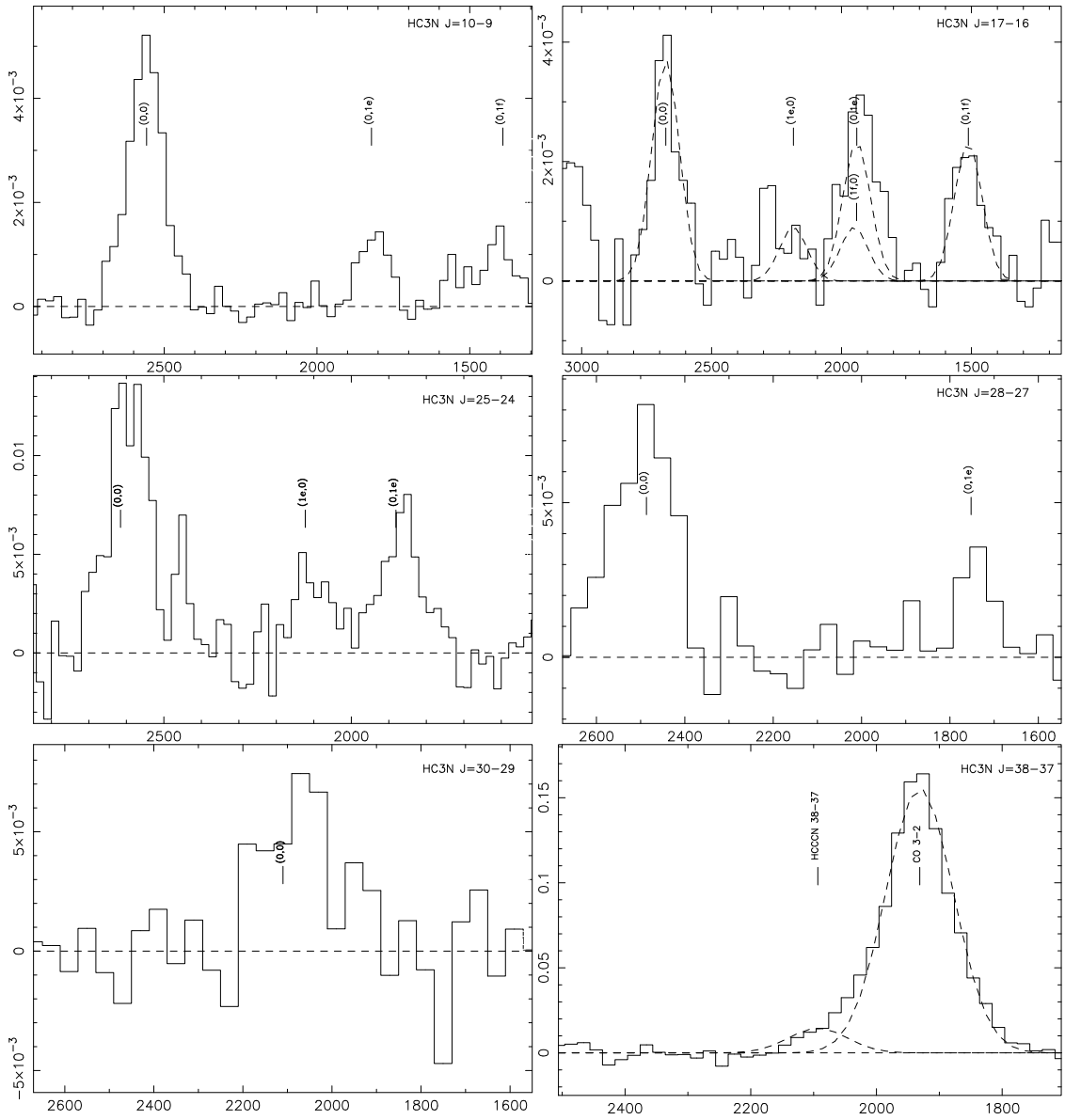

Fig. 1. Spectra of HC_3N in NGC 4418. On the X axis, the velocity scale is shown in km s^{-1}. The intensity is $T_A^\star$ in Kelvin, not corrected for main beam efficiency and beam size. The central tuning frequencies for each observed band are listed in Table 1. In the two cases *(top right, bottom right)* where significant blending is present, we show the Gaussian fits as dashed lines. See text in Sect. 3.1 for discussion about line identification.

Thanks to the relatively narrow line widths of about 120 km s^{-1}, line confusion is not a problem in most of the spectra. The most crowded situation is found in the J = 17–16 band, where multiple Gaussian fits were used to separate the v_7 = 1e and v_6 = 1f lines. Since e and f transitions come from the l-doubling of the same bending mode, we can assume that they have the same intensity. Fixing the $v_7 = 1e$ intensity to the more accurately determined $v_7 = 1f$ value (see Fig. 1), we were able to separate the $v_6 = 1f$ contribution. We note that the fitted value for $v_6 = 1f$ is consistent with the measured upper limit for the $v_6 = 1e$ line.

The molecule appears to be highly excited, with very bright emission even for large upper angular momenta and energies. After realizing this, we checked spectra of other molecules at higher frequencies to search for HC_3N contamination finding an asymmetry in the CO 3–2 spectrum at 345 GHz, taken by Monje and Aalto in 2007 with the James Clark Maxwell Telescope in Hawaii (see Fig. 1, bottom right). We interpreted this asymmetry as the HC_3N J = 38–37 line, whose fitted values are also reported in Table 1. This tentative detection was not included in our analysis.

3.2. Line widths

The observed line widths vary from 80 km s$^-$1 for the J = 28–27, v_7 = 1 transition to 182 km s^{-1} for J = 30–29. If we exclude these two extreme cases, the remaining lines show comparable line widths, with a mean value of 125 km s^{-1} and a standard deviation of 12 km s^{-1} that is smaller than the spectral resolution, which for our data is not less than 20 km s^{-1}. Line widths do not show significant trends when compared to the energy of the upper level of observed transitions and thus suggest that the emission is originating in the same dynamical region inside the galaxy. The observed line widths are comparable to those inferred from interferometric observations of other dense gas tracers, such as HCO^+ and HCN (Imanishi et al. 2004).

Table 1. Observed HC_3N Lines Properties.

Transition $J_u - J_l$ (v_6, v_7)	Rest frequency [GHz]	Tuning frequency [GHz]	HPBW[a] [″]	$\int T_A^\star dv$ [mK km s^{-1}]	T_b[b] [K]	ΔV[c] [km s^{-1}]	η_{mb}[d]	$A_{u\ell}$[e] [s^{-1}]	E_u[f] [K]	Ref.[g]
10–9 (0, 0)	90.979	91.114	27	711 ± 20	1.5	134	0.77	5.8e-05	24.1	IRAM 07-08
(1e, 0)	91.128	”	27	<70	–	–	0.77	5.8e-05	736.6	IRAM 07-08
(0, 1e)	91.202	”	27	159 ± 17	0.4	108	0.77	5.8e-05	342.6	IRAM 07-08
(0, 1f)	91.333	”	27	155 ± 14	0.4	110	0.77	5.8e-05	342.6	IRAM 07-08
16–15 (0, 0)	145.561	145.561	17	1700 ± 80	1.7	130	0.70	2.4e-04	59.4	Aalto 2007
17–16 (0, 0)	154.657	154.948	16	469 ± 52	0.5	117	0.67	2.9e-04	67.3	IRAM 07-08
(1e, 0)	155.032	”	16	<150	–	–	0.67	2.9e-04	779.2	IRAM 07-08
(0, 1e)	155.037	”	16	316 ± 59	0.3	141	0.67	2.9e-04	385.2	IRAM 07-08
(0, 1f)	155.259	”	16	316 ± 59	0.3	141	0.67	2.9e-04	385.3	IRAM 07-08
(1e, 0)	154.911	”	16	<150	–	–	0.67	2.9e-04	779.2	IRAM 07-08
25–24 (0, 0)	227.418	227.757	11	2020 ± 140	1.1	140	0.54	9.3e-04	143.0	IRAM 12-07
(1e, 0)	227.793	”	11	480 ± 110	0.3	125	0.54	9.3e-04	853.9	IRAM 12-07
(0, 1e)	227.977	”	11	928 ± 120	0.6	125	0.54	9.3e-04	459.9	IRAM 12-07
28–27 (0, 0)	254.699	254.699	10	1720 ± 100	0.9	141	0.47	1.3e-03	178.6	IRAM 12-07
28–27 (0, 0)	254.699	255.018	10	1315 ± 100	0.7	159	0.47	1.3e-03	178.6	IRAM 07-08
(1e, 0)	255.119	”	9.7	<200	–	–	0.47	1.3e-03	889.1	IRAM 07-08
(0, 1e)	255.324	”	9.7	327 ± 82	0.3	83	0.47	1.3e-03	495.2	IRAM 07-08
30–29 (0, 0)	272.884	272.884	9	1300 ± 200	0.5	182	0.44	1.6e-03	204.6	IRAM 07-08
38–37 (0, 0)	345.609	345.609	14	1930 ± 250[h]	1.8	120	0.63	3.3e-03	326.0	JCMT 2007

Notes. [(a)] Half power beam width. [(b)] Brightness temperature, assuming a 2″ source size. [(c)] Full width at half maximum from Gaussian fit. [(d)] Main beam efficiency. [(e)] Einstein's transition coefficient. [(f)] Energy above ground of the upper level. [(g)] Telescope and epoch. [(h)] From Gaussian fit to the CO 3–2 spectrum, see Fig. 1.

Unfortunately, these observations can barely resolve the 2″ emitting region and do not offer much information about the spatial distribution and dynamics of the dense gas.

It is remarkable that an edge-on galaxy exhibits these narrow emission lines. This might imply that the dense gas is mostly outside the very nuclear region. High resolution observations would help us to determine the velocity field of the central gas.

3.3. Population diagram

The observed line intensities were combined in a population diagram (see Fig. 2) to attempt a first LTE analysis of the emission. An extensive description of the population diagram method for deriving interstellar gas properties is given by Goldsmith & Langer (1999). From the basic theory of molecular emission, it can be shown that the population of a certain energy level is given by

$$N_u = \frac{8\pi k \nu^2 W}{hc^3 A_{u\ell}} \left(\frac{\tau}{1 - e^{-\tau}} \right), \quad (1)$$

where W is the integrated brightness temperature. This is related to the observed integrated $T_A^\star$ listed in Table 1 by

$$W = \int \frac{T_A^\star}{\eta_{mb}} \frac{\theta_s^2 + \theta_b^2}{\theta_s^2} dv = \frac{\theta_s^2 + \theta_b^2}{\eta_{mb} \theta_s^2} \int T_A^\star dv, \quad (2)$$

where θ_s and θ_b are the angular sizes of the source and the telescope beam respectively. In our calculations we assume $\theta_s = 2''$, which is the upper limit to the size of the HCN 1–0 emitting region found by Imanishi et al. (2004) with interferometric observations. We note that we consider source-averaged quantities, since the size of the source is much smaller than the beam and a beam-averaged approach would lead to an underestimate of the true brightness temperature and column density. Einstein's transition probability coefficients $A_{u\ell}$ were taken from the *Cologne Database of Molecular Spectroscopy*[4] (CDMS). At LTE, we have

$$N_u = \frac{N}{Z} g_u e^{-E_u/T}, \quad (3)$$

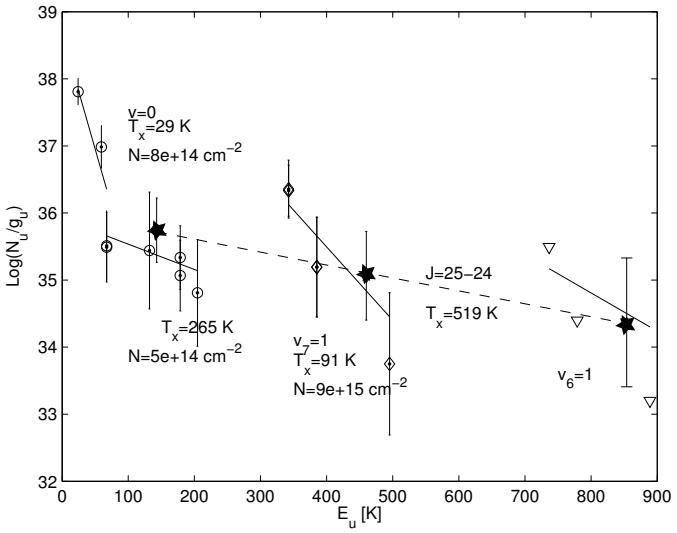

Fig. 2. Population diagram for all the observed HC_3N lines in NGC 4418. The 3-σ error bars include uncertainties in the line intensity and beam size. The solid lines represent the fit of the level population for $v = 0$ (*circles*), $v_6 = 1$ (*triangles*), and $v_7 = 1$ (*diamonds*). The dashed line fits the $v = 0$, $v_6 = 1$, and $v_7 = 1$ vibrational states of the $J = 25$ level (marked with a *star*). For the $v_6 = 1$ lines, we note that the only detection is for $J = 25$–24, the others being only upper limits. The vibrational ground state was fitted with two temperature components. The fit includes opacity corrections, as described in Appendix A. Maximum opacities are 0.04 for $v = 0$ and 0.2 for $v_7 = 1$.

[4] http://www.astro.uni-koeln.de/cdms/

where N is the total number density of molecules and Z is the partition function. For $kT > hB_0$, i.e., for warm molecular gas, we can approximate $Z \simeq kT/hB_0$, the rotational constant B_0 being 4.55 GHz for HC_3N.

Plotting the observed values of Eq. (1) versus the energy of the upper level E_u, we can find the excitation temperature of the molecule by fitting a line to the natural logarithm of Eq. (3). The excitation temperature is given by the slope of the fitted line.

The population diagram for the observed transitions is shown in Fig. 2. The line intensities were fitted using a minimum-χ^2 method. The free parameters of the fit were column density and excitation temperature, which could vary, respectively, within the ranges 10^{12}–10^{16} cm^{-2} and 10–600 K. The fit includes opacity corrections and results in an optically thin scenario, with typical optical depths of 0.04 for $v = 0$ and 0.2 for the $v_7 = 1$ transitions. A discussion about opacity effects for larger molecular column densities can be found in Appendix A.

The excitation of the molecule is described by four temperature components.

3.3.1. The rotational temperatures

The $v = 0$ levels cannot be fit by a single line and clearly exhibit two temperature components at 29 K (for $E_u < 100$ K) and 265 K (for larger E_u). The $v_7 = 1$ transitions have an excitation temperature of 91 K. These are all rotational temperatures referring to the excitation of angular momentum states of the molecule.

3.3.2. The vibrational temperature

When we compare the populations of different vibrational levels with the same J, we determine the vibrational temperature, which describes the excitation of the vibrational modes. This can be achieved for the $J = 25$–24 band, for which we have both $v_6 = 1$ and $v_7 = 1$ lines. The resulting vibrational temperature is 519 K.

The accuracy of the excitation temperatures and column densities estimated by population diagram fitting were tested by Monte Carlo simulations. These results assign a confidence limit of about 30% and 20% to the derived temperatures and column densities, respectively.

4. Discussion

In NGC 4418, the emission of HC_3N is the strongest ever detected in an extragalactic source with a HC_3N (10–9)/ HCN (1–0) line ratio of about 0.4. The excitation of HC_3N is also unusual with a large number of vibrationally excited lines detected, suggesting that the excitation of the molecule is strongly affected by radiation.

4.1. Models of the excitation of HC_3N

If we assume that HC_3N is optically thin, multiple temperature components must contribute to the emission. This is possible in a galaxy characterized by steep temperature gradients in its inner regions. We first examine how the radiation field may affect the excitation of the HC_3N molecule, and then discuss the possible origin of the temperature components.

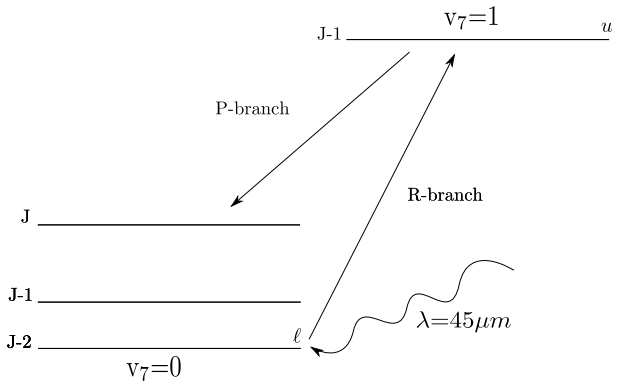

Fig. 3. Radiative pumping of HC_3N rotational levels via vibrational IR transitions.

4.1.1. IR pumping of HC_3N

The ground vibrational state of HC_3N can be excited by IR radiation at $\lambda = 45$ μm or $\lambda = 20$ μm, respectively to a $v_7 = 1$ or $v_6 = 1$ state (see Fig. 3). The excited state can then decay through the R-branch ($\Delta J = -1$) or P-branch ($\Delta J = +1$) to populate a $v = 0$ level, with a resulting selection rule $\Delta J = 2$ (Carroll & Goldsmith 1981). The level population can be estimated from Boltzmann's equation

$$\frac{n_u}{n_\ell} = \frac{B_{\ell u} I}{B_{u\ell} I + A_{u\ell}} = \frac{g_u}{g_\ell} e^{-\frac{h\nu}{kT}}, \tag{4}$$

where ℓ and u refer respectively to the ground and excited vibrational state. Assuming $g_\ell B_{\ell u} = g_u B_{u\ell}$, the maximum pumping rate is given by

$$B_{\ell u} I = \frac{A_{u\ell}}{e^{\frac{h\nu}{kT}} - 1} \equiv P_{\ell u}. \tag{5}$$

This has to be compared to the collisional excitation rate $C_{J-1\to J} = n(H_2) q_{J-1\to J}$ for the rotational levels of the ground vibrational state. The previous formula gives an upper limit for the *pumping critical density* of $n_{cp} = P_{\ell u}/q_{J-1\to J}$.

For $n(H_2) < n_{cp}$ the radiative pumping process is more efficient than collisions in exciting the molecule.

The collisional coefficients $q_{J-1\to J}$ of the first 20 rotational levels of HC_3N, for different gas temperatures, can be found in the Leiden Atomic and Molecular Database. We considered an impinging IR flux coming from an optically thick dust source at 85 K. We used this temperature for determining both pumping rates and collisional coefficients. Typical pumping rates are of the order of 10^{-5} s^{-1} for both $\lambda = 20$ μm and $\lambda = 45$ μm across all the range of upper state angular momenta. The collisional coefficients at 85 K do not show significant variations for different transitions and have a value of about 10^{-10} cm^{-3} s^{-1}. The resulting pumping critical density is $n_{\rm cp} \simeq 10^5$ cm^{-3}. The density structure of the HC_3N emitting gas in NGC 4418 remains unknown and therefore we cannot provide a quantitative estimate of the impact of pumping on the ground state rotational levels. However, for a clumpy medium where dense clouds are surrounded by low-density diffuse molecular gas, the pumping would act directly on the diffuse medium raising the global intensity and rotational temperature of the emission.

4.1.2. The cool, 30 K, and warm 90 K components

The 90 K rotational temperature of the v_7 bending ladder may originate in dense gas within the inner 0.5″. The dust

Table 2. Excitation properties of HC_3N bending modes from Wyrowski et al. (1999).

Transition	λ_{ex} [μm]	$A_{u\ell}$ [s^{-1}]	n_{cr} [cm^{-3}]	Vibration
v_6 = 1–0	20	0.15	3×10^{11}	CCN bend
v_7 = 1–0	45	6×10^{-4}	4×10^{8}	CCC bend

Notice the large critical densities, see discussion in the text.

temperature of 85 K found by Evans et al. (2003) agrees well with the rotational temperature, which may be because either the IR radiation field dominates the excitation, or the gas and dust are in thermal equilibrium and the rotational temperature reflects the gas kinetic temperature.

The low temperature, 30 K, component could be coming from a more extended phase, at a greater distance from the warm dust in the center. The existence of this cool component is inferred from the lower transition $v = 0$ lines and can be confirmed by observations of low-J lines with, for example, the Effelsberg telescope.

4.1.3. The hot, 260 K and 500 K, components

As we can see in Fig. 2, the estimated rotational temperature of the high-J transitions is higher than the 30 K found for the low-Js, by almost one order of magnitude. This change in the slope of the rotational diagram cannot be explained by opacity effects and must be investigated further. Concave population diagrams are commonly found in Galactic molecular observations and are often attributed to multiple temperature layers. Temperatures of 300 K are typical of Galactic hot cores around sites of massive star formation (see Sect. 4.4), the excitation temperature found could thus be reflecting the true gas kinetic temperature. This is in agreement the detections of the 14 μm absorption of HCN, for which Lahuis et al. (2007) find gas temperatures of about 300 K in the core of NGC 4418.

The vibrational temperature of the J = 25–24 lines is about 500 K. The bending modes v_6 and v_7 both have critical densities greater than 10^8 cm^{-3} (see Table 2) and are thus probably radiatively excited. The derived vibrational temperature then reflects the temperature of a radiation field.

4.1.4. Radiative excitation of high-J levels

The high temperature of the high-J rotations may also be caused by radiative excitation, that becomes more and more efficient as the angular momentum of the upper state increases. The critical density of a $J \rightarrow J-1$ transition can be written as

$$n_c = \frac{A_{J,J-1}}{q_{J,J-1}} = \frac{64\pi^4}{3hc^3}\nu^3\mu^2\frac{J+1}{2J+3}\frac{1}{q_{J,J-1}}, \quad (6)$$

where ν is the line frequency and μ is the electric dipole moment of the molecule. For $n(H_2) < n_c$, the excitation temperature is determined by the radiation field and not the gas kinetic temperature. The critical densities of the first 20 rotational transitions of HC_3N are shown in Fig. 4. We see that n_c increases from 10^3 cm^{-3} for $J_u = 1$ to more than 10^6 cm^{-3} for $J_u = 20$. For $J_u > 15$, we note that the critical density is higher than 10^6 cm^{-3}. This region corresponds to energies E_u greater than 100 K, which is the critical value at which the population diagram of Fig. 2 exhibits a change in slope towards higher

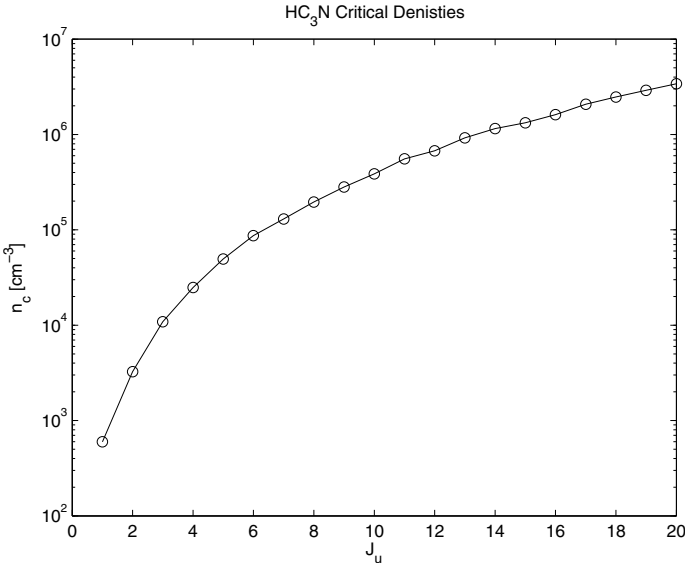

Fig. 4. Critical densities for the first 20 rotational levels of HC_3N. Emission and collisional coefficients from Leiden Atomic and Molecular Database.

excitation temperatures. For $n(H_2) < 10^6$, this may imply that the excitation of high-J levels is affected considerably by continuum radiation.

4.1.5. Can the 500 K component exist?

Infrared observations by Evans et al. (2003) report a dust temperature of 85 K. This value was inferred by comparing the IR fluxes at 60 and 100 μm, and can be combined with the total IR flux to estimate the size of the emitting region. In their paper, Evans and collaborators find an optically thick dust source of about 0.5″ in size, corresponding to 70 pc at a distance of 30 Mpc.

Assuming that our 500 K component also represents the temperature of the IR continuum, the required source size θ for the emitting region can be estimated by the relation $L_{mIR} \propto \theta^2 T^4$, which infers $\theta = 0.01''$. This corresponds to a linear diameter of 1.45 pc. This is an upper limit to the size of the emitting region, where it is the origin of all the observed IR flux. Our interpretation of the molecule's excitation then implies that an extremely compact radiation source exists in the core of NGC 4418. This may correspond to a deeply embedded AGN, heating the surrounding high column of dust to the required high temperatures. A hot 500 K component would peak at 10 μm, right on top of the silicate absorption band, which in NGC 4418 is one of the deepest ever measured in a luminous IR galaxy (Spoon et al. 2007). This high temperature feature might be hidden in the silicate dip and not be evident in the SED. Furthermore, Lahuis et al. (2007) find gas temperatures from the 14 μm absorption of HCN to be 300 K in the core of NGC 4418. This would require the continuum source to be hotter than 300 K gas observed in absorption.

4.2. Models of the excitation of HC_3N – optically thick case

If we abandon the notion that HC_3N is optically thin, we show in Appendix A that optical depth effects may allow us to fit a single temperature (with however significant scatter) to the $v = 0$ transitions. This lowers the excitation temperature of the high-J

levels, but leaves us with extreme column densities of HC_3N and large optical depths that should result in strong lines in the ^{13}C isotopic variants of HC_3N.

Assuming a Galactic C/^{13}C abundance ratio, these lines should have intensities comparable to the emission of the main isotopomer. However, measurements of the 3 mm band obtained using the new EMIR receiver at IRAM 30 m (Costagliola et al., in prep.) show that the emission from H^{13}CCCN J = 10–9 is at least 10 times fainter than that from the main ^{12}C variant. Even when attempting to correct for optical depth effects, we still have trouble fitting all the points to a single temperature and the column densities required ($N(HC_3N) > 10^{17}$ cm^{-2}) imply HC_3N abundances in excess of those of HCN and HCO$^+$, starting to approach those of CO.

4.3. HC_3N abundance

From the population diagram in Fig. 2, the v_7 component has a column density of 8.7×10^{15} cm^{-2}, which can be assumed to be a lower limit to the total HC_3N column.

The hydrogen column is estimated from ^{13}CO J = 1–0 and J = 2–1 measurements, taken in 2007 and 2008 at IRAM 30 m (Costagliola et al., in prep.). A basic LTE interpretation of ^{13}CO intensities leads to a source-averaged column density $N(^{13}CO) \simeq 5.2 \times 10^{16}$ cm^{-2}. Assuming a C/^{13}C ratio of 50, typical of starburst galaxies (e.g., Henkel & Mauersberger 1993; Mao et al. 2000) and applying a $N(CO)/N(H_2) = 10^{-4}$ conversion (Blake et al. 1987), we obtain a molecular hydrogen column $N(H_2) \simeq 2.6 \times 10^{22}$ cm^{-2}. This estimate is consistent with the value of 7.7×10^{22} cm^{-2} derived by Lahuis et al. (2007) from silicate absorption in *Spitzer* spectra. The resulting HC_3N abundance is then $X[HC_3N] = N(HC_3N)/N(H_2) = 3.4 \times 10^{-7}$.

In our calculations we assume that the ^{13}CO emission is optically thin and effectively traces the hydrogen column. The observed ^{12}CO/^{13}CO J = 1–0 ratio in this galaxy is about 20, implying only moderate ^{12}CO opacities. It is therefore reasonable to assume optically thin emission for ^{13}CO.

4.4. HC_3N in the Galaxy

In our Galaxy, HC_3N is often associated with hot cores, i.e., dense and warm regions around newborn massive OB stars. Here, large dust columns ($A_V \simeq 1000$) provide shielding against UV radiation from the central object. The first interstellar detection of vibrationally excited HC_3N was by Clark et al. (1976) toward the Orion hot core and an extensive survey of vibrationally excited lines in other Galactic sources was performed by Wyrowski et al. (1999). Bright HC_3N emission has also been found towards circumstellar envelopes and regions around planetary nebulae (Pardo et al. 2004).

Our estimate of the HC_3N abundance has the same order of magnitude as that found by de Vicente et al. (2000) towards hot cores in Sgr B2, one of the most active regions of high mass star formation in the Milky Way. An enhancement of HC_3N abundance in hot cores was also observed in Orion A (Rodriguez-Franco et al. 1998), where the abundance is higher by about one order of magnitude than that of the diffuse warm gas, reaching values close to 10^{-8}. In the same complex, HC_3N strongly anticorrelates with HII regions, where it is likely to be destroyed by the strong UV radiation.

The estimated HC_3N abundance for NGC 4418 thus resembles the properties of Galactic hot cores, where the highest concentration of the molecule has been observed. It is quite remarkable that this appears to be a global property of the galaxy, especially considering that ^{13}CO emission might be more extended than HC_3N and thus the estimated abundance might be only a lower limit to its true value.

4.5. HC_3N in other galaxies

One reason for selecting NGC 4418 to perform a deeper study of its HC_3N component was the unusual luminosity of its HC_3N 10–9 line. Combining observational data with data in the literature, Lindberg (2009) classified galaxies as *HC_3N-luminous* when the HC_3N 10–9 line was at least 15% of the HCN 1–0 line intensity. He found that only a few (5) of 30 galaxies in his sample fitted this category. NGC 4418 belongs to this exclusive class of HC_3N-luminous objects, having an HC_3N/HCN line intensity ratio of 0.4. In a high resolution study of IC 342, Meier & Turner (2005) find that HC_3N emission correlates well with the 3 mm continuum emission, and avoids regions of high UV radiation. For example, they find a spatial anticorrelation between HC_3N and the PDR-tracer C_2H. The conclusion is that HC_3N traces young star-forming regions. On the scale of the main molecular complexes, the HC_3N/HCN ratio is 0.28, which is still lower than the global value for NGC 4418. Wang et al. (2004) report a summary of HC_3N abundances in the nearby starbursts NGC 253 and M 82 as well as the Seyfert-2 NGC 4945, where these range from $X = 10^{-9.0}$ to $10^{-7.9}$. For these three galaxies, Lindberg lists the HC_3N/HCN intensity ratio to be less than 0.1 for NGC 253 and NGC 4945 and for M 82 it is less than 0.2. We note that these are central and not global ratios, these three galaxies being extended compared to the single-dish beam.

4.6. Outlook

To confirm the presence of a 260 K component, we need carefully calibrated submm data of the high-J transitions. To more tightly constrain the excitation and spatial extent of HC_3N, high resolution interferometric observations are important. A hot, 500 K, dust component should be identifiable by high resolution IR observations.

In a previous paper we proposed that HC_3N could be used as an indicator of AGN since HC_3N should be destroyed by both ions and UV radiation. In a follow-up paper, we will present models of the impact of XDRs and PDRs on the HC_3N abundances and discuss the survival and formation of HC_3N in these environments. We do not discuss in this paper the possibility that the hot component is not excited by a radiation source, but that the temperature instead reflects the formation and destruction processes of HC_3N, thus indicating that they must be taken into account when modeling the excitation of the molecule. We are aware of the fact that a non-LTE analysis would be required to properly address the problem of the molecule's excitation. A complete analysis of the excitation and the chemistry of HC_3N will be discussed in a follow-up paper.

5. Conclusions

We have confirmed the first extragalactic detection of vibrational lines of HC_3N. We have detected 6 different rotational transitions ranging from J = 10–9 to J = 30–29 in the ground vibrational state, plus a tentative detection of the J = 38–37 line. We have also detected 7 rotational transitions of the vibrationally excited states v_6 and v_7, with angular momenta ranging from J = 10–9

to 28–27. In the optically thin regime, we find that the $v = 0$ transitions can be reproduced by models of two temperatures, 29 K and 265 K, while the v_7 lines can be fitted by a temperature of 91 K. The vibrational temperature, fitted to the $J = 25$–24 transitions is, 519 K. By allowing the column density to vary between the different temperature components, we inferred HC_3N column densities of 8×10^{14} cm^{-2} for the vibrational ground level, and 9×10^{15} cm^{-2} for the vibrational $v_7 = 1$ transitions.

The excitation of the HC_3N molecule responds strongly to the intense radiation field and the presence of warm, dense gas and dust at the center of NGC 4418. The intense HC_3N line emission is a result of both high abundances and excitation. The HC_3N excitation and abundances seem similar to those found for hot cores in Sgr B2 in the Galactic Center. This implies that the nucleus of NGC 4418 has properties in common with Galactic hot cores. It cannot be excluded that the hot (500 K) component may be associated with a buried AGN.

Acknowledgements. We thank the staff at the IRAM 30 m telescope for their kind help and support during our observations. Furthermore, we would like to thank the IRAM PC for their generous allocation of time for this project.
This research was supported by the EU Framework 6 Marie Curie Early Stage Training programme under contract number MEST-CT-2005-19669 "ESTRELA" and by the European Community Framework Programme 7, Advanced Radio Astronomy in Europe, grant agreement No. 227290, "RadioNet".

Appendix A: Opacity effects

The effects of a finite optical thickness of the observed lines on the population diagram have been investigated by different authors, e.g., Goldsmith & Langer (1999) and Wyrowski et al. (1999).

If we were to define $C_\tau = \tau/(1 - e^{-\tau})$ as the correction due to optical depth, Eq. (1) would read

$$N_u = \frac{8\pi k\nu^2 W}{hc^3 A_{u\ell}} C_\tau \equiv N^{\rm thin} C_\tau. \quad \text{(A.1)}$$

For $\tau \ll 1$, $C_\tau \simeq 1$ and $N_u \simeq N^{\rm thin}$, but for $\tau > 1$, we have $C_\tau \simeq \tau$ and the observed line intensities lead to an underestimate of the derived column density if no correction is applied.

For a linear molecule, the optical depth of a $J \rightarrow J - 1$ transition is given by

$$\tau = \frac{8\pi^3\mu^2}{3h} \frac{N}{Z\Delta v} J e^{-\alpha J(J+1)} \left(e^{2\alpha J} - 1\right), \quad \text{(A.2)}$$

where μ is the dipole moment of the molecule and $\alpha \equiv hB_0/kT_{\rm ex}$, where B_0 is the rotational constant. If $kT_{\rm ex} \gg hB_0$, the partition function can be approximated by $Z \simeq \alpha^{-1}$ (Goldsmith & Langer 1999). This is often the case for HC_3N in interstellar space, since $B_0 = 4.55$ GHz and the previous condition becomes $T_{\rm ex} \gg 0.2$ K.

The lack of detected emission from ^{13}C-variants of HC_3N (see Sect. 4.2) prevents us from obtaining a direct estimate of the optical depth. We therefore used Eqs. (A.1) and (A.2) to fit the observed intensities via a minimum-χ^2 method. We focused in particular on the $v = 0$ lines, to find out whether the change in slope could be due to optical depth effects rather than a high-temperature population. The result of the fit is shown in Fig. A.1. The free parameters were excitation temperature, column density, and source size, which were varied across a wide range of values.

We obtain two possible solutions, one at $N = 8.3 \times 10^{14}$ cm^{-2} and one at $N > 10^{17}$ cm^{-2}. Both panels in Fig. A.1 show that a single component does not fit the observed intensities. When we reach the optically thick regime (around 10^{16}–10^{17} cm^{-2}) the fit improves very slowly with increasing column density. However, even for extremely large columns (e.g. 10^{25} cm^{-2}), the normalized χ^2 is still high (around 20). Thus the change in slope of the population diagram cannot be explained by optical depth effects.

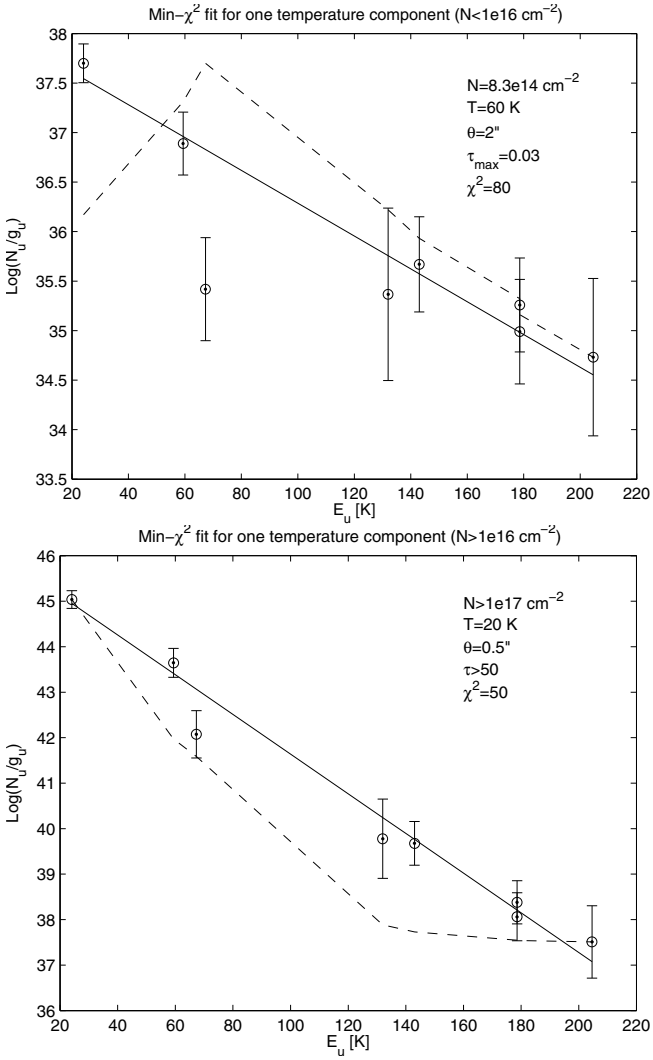

Fig. A.1. Fit of HC_3N $v = 0$ intensities including optical depth effects. *Top*: fit for HC_3N column density smaller than 10^{16} cm^{-2} (normalized $\chi^2 = 80$). *Bottom*: fit for HC_3N column density larger than 10^{16} cm^{-2} (normalized $\chi^2 = 50$). In both fits, the source size θ could vary between 0.1 and 2 arcsec. The dashed line represents the optical depth for the different transitions, in arbitrary units.

An estimate of the optical depth of the observed lines can be obtained by comparing their brightness temperature ($T_{\rm b}$ in Table 1) to the excitation temperature. In general, for a spectral line we have $T_{\rm b} = (T_{\rm ex} - T_{\rm B})(1 - e^{-\tau})$. Neglecting the contribution from the background $T_{\rm B}$, the optical depth is given by $\tau = -\ell{\rm n}(1 - T_{\rm b}/T_{\rm ex})$. Considering an excitation temperature of 30 K for the first three $v = 0$ lines in Table 1, we derive $\tau < 0.06$, which is consistent with our optically thin scenario.

References

Aalto, S., Polatidis, A. G., Hüttemeister, S., & Curran, S. J. 2002, A&A, 381, 783
Aalto, S., Monje, R., & Martín, S. 2007, A&A, 475, 479

Baan, W. A., Henkel, C., Loenen, A. F., Baudry, A., & Wiklind, T. 2008, A&A, 477, 747
Blake, G. A., Sutton, E. C., Masson, C. R., & Phillips, T. G. 1987, ApJ, 315, 621
Brown, J. M., Hougen, J. T., Huber, K. P., et al. 1975, J. Mol. Spect., 55, 500
Carroll, T. J., & Goldsmith, P. F. 1981, ApJ, 245, 891
Clark, F. O., Brown, R. D., Godfrey, P. D., Storey, J. W. V., & Johnson, D. R. 1976, ApJ, 210, L139
de Vicente, P., Martín-Pintado, J., Neri, R., & Colom, P. 2000, A&A, 361, 1058
Downes, D., & Eckart, A. 2007, A&A, 468, L57
Evans, A. S., Becklin, E. E., Scoville, N. Z., et al. 2003, AJ, 125, 2341
Gao, Y., & Solomon, P. M. 2004, ApJS, 152, 63
Goldsmith, P. F., & Langer, W. D. 1999, ApJ, 517, 209
Graciá-Carpio, J., García-Burillo, S., Planesas, P., Fuente, A., & Usero, A. 2008, A&A, 479, 703
Guesten, R., Serabyn, E., Kasemann, C., et al. 1993, ApJ, 402, 537
Henkel, C., & Mauersberger, R. 1993, A&A, 274, 730
Imanishi, M., Nakanishi, K., Kuno, N., & Kohno, K. 2004, AJ, 128, 2037
Imanishi, M., Nakanishi, K., Tamura, Y., Oi, N., & Kohno, K. 2007, AJ, 134, 2366
Krips, M., Neri, R., García-Burillo, S., et al. 2008, ApJ, 677, 262
Lahuis, F., Spoon, H. W. W., Tielens, A. G. G. M., et al. 2007, ApJ, 659, 296
Lindberg, J. 2009, Master's Thesis at Chalmers University of Technology, Sweden
Mao, R. Q., Henkel, C., Schulz, A., et al. 2000, A&A, 358, 433
Meier, D. S., & Turner, J. L. 2005, ApJ, 618, 259
Meijerink, R., Spaans, M., & Israel, F. P. 2007, A&A, 461, 793
Monje, R. R., & Aalto, S. 2008, in EAS Publ. Ser. 31, ed. C. Kramer, S. Aalto, & R. Simon, 81
Pardo, J. R., Cernicharo, J., Goicoechea, J. R., & Phillips, T. G. 2004, ApJ, 615, 495
Rodriguez-Franco, A., Martin-Pintado, J., & Fuente, A. 1998, A&A, 329, 1097
Roussel, H., Helou, G., Beck, R., et al. 2003, ApJ, 593, 733
Sanders, D. B., & Mirabel, I. F. 1996, ARA&A, 34, 749
Spoon, H. W. W., Keane, J. V., Tielens, A. G. G. M., Lutz, D., & Moorwood, A. F. M. 2001, A&A, 365, L353
Spoon, H. W. W., Marshall, J. A., Houck, J. R., et al. 2007, ApJ, 654, L49
Viti, S., & Bayet, E. 2008, in EAS Publ. Ser. 31, ed. C. Kramer, S. Aalto, & R. Simon, 57
Wang, M., Henkel, C., Chin, Y., et al. 2004, A&A, 422, 883
Wyrowski, F., Schilke, P., & Walmsley, C. M. 1999, A&A, 341, 882
Yamada, K. M. T., & Creswell, R. A. 1986, J. Mol. Spect., 116, 384